

---

# Island wakes in the Southern California Bight

---

Rui M.A. Caldeira<sup>1</sup>, Patrick Marchesiello<sup>2</sup>,  
Nikolay P. Nezlin, Paul M. DiGiacomo<sup>3</sup>  
and James C. McWilliams<sup>2</sup>

## ABSTRACT

In this study, we investigated wind-induced and current-induced island wakes, using a multi-platform approach of *in situ*, remote sensing, and numerical model simulations for the Southern California Bight (SCB). Island wind wakes are a result of sheltering from the wind, with weak wind mixing, strong heat storage, and consequent high sea surface temperature (SST). Wind wakes around Santa Catalina Island are most persistent during spring and summer months. Current wakes, caused by the disruption of the poleward traveling California Counter Current, induce eddies to form off the north end of Santa Catalina Island and these move poleward every nine to twelve days. Current wake eddies induce strong mixing, with low SST and high-density sea surface signatures, whereas wind wakes induce high sea surface temperature signatures associated with the formation of a well-defined shallow thermocline. Current wake eddies vary from 1 - 30 km in diameter. From numerical solutions we predicted the frequency of occurrence of current induced wakes, off Santa Catalina Island. Wind wakes were also observed off all the other islands of the SCB as seen from the analysis of Synthetic Aperture Radar data. Time-series analysis of the island-mass-effect phenomenon has shown a concurrence of low SST and high sea surface chlorophyll for Santa Catalina, San Nicholas, and San Clemente Islands that might be related to the seasonality of the California Current and California Counter Current. Future oceanographic research in the SCB should not ignore the occurrence of wind-and current-induced island features, because they may be important in the transport and/or retention of nutrients, pollutants and plankton.

## INTRODUCTION

Island wakes have been intensively studied. The term has been used to refer to wind-induced wakes

formed on the leeward side of islands due to the sheltering from the wind with concomitant weaker mixing and warm sea surface temperatures (SST). Current wakes are formed when bathymetry defects incoming ocean currents with eddy formation and upwelling of cool deep water often associated with high productivity. It is important that wind wakes on the sea surface not be confused with atmospheric wind wakes on the lee of an island, such as atmospheric Von Karman Vortex Streets (e.g., Caldeira *et al.* 2002). We use the term wind wakes here to refer to the effect of the wind on sea surface thermal-patterns caused by the sheltering from the island's orography.

Island wakes are also related to the "island mass effect". The island mass effect concept was first described by Doty and Oguri (1956) as an increase in "biological productivity," i.e., chlorophyll concentration, on the east side of Oahu Island in the Hawaiian Archipelago. Subsequently, the effect of island bathymetry on ambient oceanography was generalized to include island effects around entire islands (Hamner and Hauri 1981a), and island mass effects now include differences in phytoplankton, zooplankton, and fish biomass due to the formation of island-induced wakes, eddies, fronts, filaments, and upwelling processes (Hernandez-Leon 1988, 1991; Aristegui *et al.* 1994, 1997; Rissik *et al.* 1997).

Owen (1980) first identified eddy-like motions offshore of Santa Catalina Island. Sea surface drogue trajectories showed trapping and circular motions to the southeast side of Santa Catalina Island, but no mention was made of the formation of a possible current wake. In fact, most oceanographic characterizations of the Southern California Bight (SCB) thereafter have not been concerned with the small-scale circulation around the islands (Bray *et al.* 1999; Hickey 1979, 1991, 1992, 1993, 1998). Most recently, DiGiacomo and Holt (2001), have described an abundance of small-scale eddies (less than 50 km) induced by the

---

<sup>1</sup>University of California, Los Angeles, Marine Science Center Los Angeles, CA

<sup>2</sup>University of California Los Angeles, IGPP, Los Angeles, CA

<sup>3</sup>California Institute of Technology, Jet Propulsion Laboratory, Pasadena, CA

island and coastline bathymetry occurring in the San Pedro, Santa Catalina, and Santa Barbara Basins.

Studies on both wind and current induced island wakes have been carried out around the Canary Island Archipelago (Aristegui *et al.* 1994, 1997; Barton *et al.* 1998, 2000). Barton *et al.* (2000) clearly distinguished cyclonic and anticyclonic current eddies downstream of Gran Canaria (Canary Islands), from warm surface wind-induced wakes leeward of the island using SST from satellite images.

Our study in the SCB investigates the differences between island wakes induced by the wind and island wakes induced by ocean currents flowing past the island's shelf. It is an expansion on the brief discussion of these issues presented in Caldeira and Marchesiello (2002). It is also an attempt to characterize the biological consequences, or island mass effect of these wakes. We also focus on the historically overlooked discussion on submesoscale circulation patterns (<10 km) around the SCB. First, we start by setting the historical oceanographic scenarios for the region. Second, we use a case study around Santa Catalina Island to distinguish between wind- and current-induced island wakes, using *in situ*, remote sensing, and numerical modeling data. Third, we expand our description of island wakes to include observations of other islands of the SCB. Lastly, we attempt to quantify the island mass effect using a time series analysis from Sea-viewing Wide Field-of-view Sensor (SeaWiFS) derived sea surface chlorophyll and Advanced Very High Resolution Radiometer (AVHRR) SST data.

## Geographic setting

South of Point Conception (PC) the coastline forms a basin referred to as the SCB (Figure 1). The SCB consists of a set of basins separated by islands and underwater ridges. It is bordered by a narrow shelf 3 to 6 km wide, mostly shallower than 50 m. The basins between ridges are rather deep (>500 m). The stream of the California Current (CC) turns to south-southeast and passes along the continental slope. At approximately 32°N a branch of the CC turns eastward and then northward along the coast of the SCB, forming a large gyre known as the Southern California Eddy (SCE). The poleward traveling current along the coast is known as the California Counter Current (CCC) and transports warm water, often poor in chlorophyll, into the Santa Monica Basin (SMB) and the Santa Barbara Channel. At the northwestern end of SMB, the poleward flow divides into two flows: one flow-

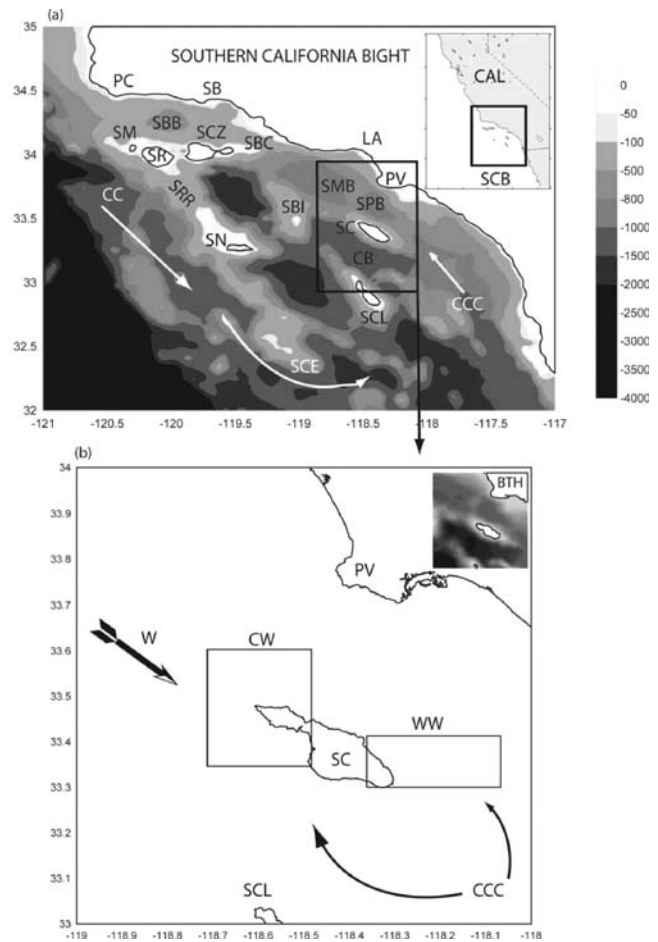


**Figure 1. (Top) Various locations in the Southern California Bight (SCB) map. California (CAL); Point Conception (PC); Santa Barbara (SB); Los Angeles (LA); Palos Verdes Peninsula (PV); San Miguel Island (SM); Santa Rosa Island (SR); Santa Rosa Ridge (SRR); Santa Cruz Island (SCZ); Santa Barbara Basin (SBB); Santa Barbara Channel (SBC); Santa Barbara Island (SBI); San Nicolas Island (SN); Santa Monica Basin (SMB); San Pedro Basin (SPB); Santa Catalina Island (SC); Catalina Basin (CB); San Clemente Island (SCL); California Current (CC); Southern California Eddy (SCE); California Counter Current (CCC). (Bottom) California Counter Current (CCC) reaching Santa Catalina Island (SC) forming a current-induced wake (CW) to the north; Opposite Wind (W) causing a wind-induced wake (WW) leeward of Catalina (to the southeast) and detail of the bathymetry (BTH) is for the same region.**

ing northwestward through the Santa Barbara Channel, and the other flowing westward to the south of the Channel Islands (Sverdrup and Fleming 1941, Lynn and Simpson 1987, Hickey 1992, Bray *et al.* 1999).

The intensity of the CC System varies seasonally. During winter and summer the poleward transport of the CCC intensifies and the jet of the

CC migrates offshore, while warm southern waters penetrate further to the north and west within the SCB (Reid and Mantyla 1976, Hickey 1979, Bray *et al.* 1999, Haney *et al.* 2001).

The strongest equatorward winds occur during spring along most of the California Coast (Hickey 1998). Also during spring the CC is closer to shore and becomes increasingly jet-like, with predominantly equatorward flow in the SCB. Winds in the SCB are generally weaker than north of PC, with significant daily and seasonal fluctuations. In general, the correspondence between ocean current transport and wind stress and/or curl is not particularly good for the SCB. However, one exception is that in spring, equatorward anomalies in ocean current transport near the coast are associated with equatorward wind stress anomalies as would be expected from coastal upwelling. Another correspondence is that positive curl in the average wind fields, approximately 200 km inshore, is associated with poleward ocean flow. Northwestern wind dominates year round (offshore). During winter the wind direction is more variable; from March to November northwesterly wind is steadier. Maximum wind speed is observed in spring decreasing during summer months (Bray *et al.* 1999).

Santa Catalina Island is located in the SCB at 33.3°N 118.3°W. The island is 33.7 km long by 11.7 km at its widest part. The island stands on its own shelf, 32 km offshore from the Palos Verdes Peninsula and 31 km from San Clemente Island (Figure 1). The San Pedro Basin, located between Santa Catalina Island and the mainland, reaches depths of 880 m. The Catalina Basin, between Santa Catalina Island and San Clemente Island, reaches depths of 1200 m. Santa Catalina Island has a ridge of mountains extending from northwest to southeast, seen in the Synthetic Aperture Radar (SAR) image (Figure 2a), that can reach 640 m above sea level.

An ERS-1 SAR image acquired 28 May, 2004, illustrates some of the submesoscale complexity in the Santa Catalina Island and San Pedro Basin region. A current wake with spiral eddies was detected to the northwest of Santa Catalina Island, whereas to the east, sheltered from the mountain range, there was a wind-induced wake forming (see dark patch of reduced backscatter in Figure 2a). A spiral eddy ~10 km in diameter and cyclonic in rotation is visible off the northwest end of Santa Catalina Island (CWE), as is a wind wake (WW) off

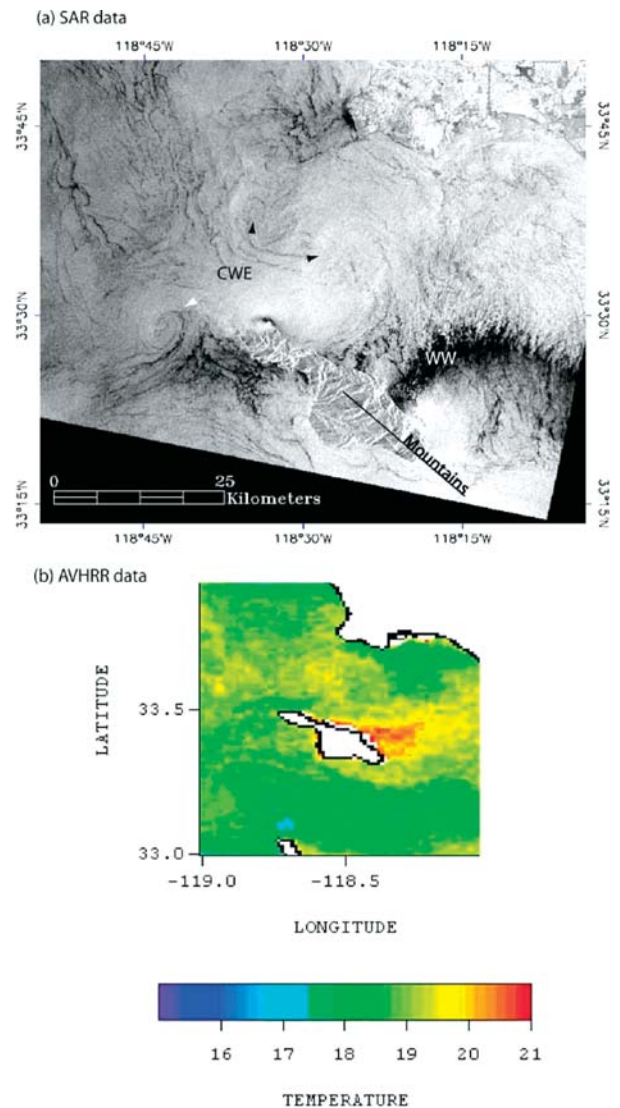


**Figure 2.** ERS-1 Synthetic Aperture Radar (SAR) image acquired May 28, 1994 at 18:34 UTC (a). AVHRR data collected on May 29 (00:38 UTC; b).

the island's eastern end. Other features are visible in the channel adjoining the mainland. Copyright ESA 1994. AVHRR data from the next day clearly showed the sea surface signature of warm water in the wind wake region (21°C), whereas north of the island the waters at the surface were 18°C (Figure 2b). A warm wind-induced wake is visible in the lee of Catalina.

## METHODS

### Data

#### SAR data

SAR imagery provides fine-resolution active microwave observations of sea-surface roughness

not affected by cloud cover or availability of light. Factors modulating sea-surface roughness include wind, interactions of waves/currents, and the presence of oils and surfactants on the ocean surface. Variability in observed surface roughness (~backscatter) can be used to visualize numerous dynamic oceanographic and boundary layer features, e.g., fronts and eddies (Munk *et al.* 2000 DiGiacomo and Holt 2001) atmospheric waves and wind shadowing (Clemente-Colon and Yan 2000) and pollution hazards (DiGiacomo *et al.* 2004). The ERS-1 and ERS-2 (hereafter ERS-1/2) SAR data utilized in this study were obtained from the European Space Agency (ESA); images were acquired at the receiving station operated by the Canada Centre of Remote Sensing in Prince Albert, Saskatchewan. The Canadian Space Agency's RADARSAT SAR data used here were received by the same Prince Albert Receiving Station and processed at the Alaska Satellite Facility, located at the University of Alaska in Fairbanks, Alaska. RADARSAT data were also acquired via an onboard tape recorder. The ERS-1/2 and RADARSAT SAR instruments all operate at a C-band frequency of 5.3 GHz, but differ in polarization: vertical transmit-vertical receive (VV) for ERS-1/2 and horizontal transmit-horizontal receive (HH) for RADARSAT. Data were obtained in one of two configuration modes: 1) standard beam mode for both ERS-1/2 and RADARSAT which has a swath width of 100 km, a pixel size of 12.5 m (averaged to 100 m here), and operates over varying fixed ranges of incidence angles; and 2) for RADARSAT only, the ScanSAR Wide-beam B mode, which has a swath width of 450 km over incidence angles from 20 - 47° and a 100-m pixel size in the imagery presented here.

#### *AVHRR SST data*

The daily satellite images of SST were obtained from the CoastWatch program. SST was measured by AVHRR on the National Oceanic and Atmospheric Administration (NOAA)-series polar-orbiting meteorological satellites. The AVHRR sensor measured radiance from the ocean surface in five near-infrared and infrared channels with 1.1-km spatial resolution at nadir. Satellite images were processed at NOAA CoastWatch data center. SST estimates were made by converting the radiance measured in the infrared channels to brightness temperature and then using a multichannel technique (McClain *et al.* 1985) to calculate SST to within

±0.5° C. Cloud identification masks were created using visible and infrared channels with a series of spectral gradient, difference, and threshold tests.

#### *Wind data*

Wind data were obtained from the Coupled Ocean/Atmosphere Mesoscale Prediction System (COAMPS) from the Naval Research Laboratory (NRL). COAMPS uses a 9-km mesh grid in the SCB nested within 27 km grid spacing. COAMPS includes automated complex quality control software, a multivariate optimum interpolation atmospheric analysis, and the COAMPS Ocean Data Assimilation System. The NRL Coupled Ocean/Atmosphere Mesoscale Prediction System-On Scene (COAMPS-OS) is an automated, portable, atmospheric nowcast/forecast data assimilation system. COAMPS-OS allows us to independently assimilate local observations, satellite-derived observations, and boundary conditions for a regional center; and to maintain data assimilation, nowcast, and a forecast capability. In order to study seasonal wind variability, the data were averaged for each month of the year, from October 1, 1998, to September 30, 2000, so that persistent wind patterns would be revealed. Wind stress ( $\tau = \rho_a C_D W^2$ ) was plotted overlaying gradients of calculated Ekman depths ( $D_E = 0.7 u^*/f$ ), where  $u^*$  is the friction velocity proportional to the wind;  $f$  is the Coriolis parameter;  $\rho_a$  is the density of air;  $C_D$  is the non-dimensional drag coefficient ( $\sim 1.4 \times 10^{-3}$ ); and  $W$  is the wind speed in  $\text{ms}^{-1}$ .

#### *In situ data*

*In situ* data were acquired aboard the University of California, Los Angeles (UCLA) Marine Science Center R/V Sea World. Twenty-four stations were visited in a grid distributed around Santa Catalina Island (see Figure 3a for station locations). At each station measurements of position, water visibility, wind speed and direction were taken. Conductivity-Temperature-Depth (CTD) casts and plankton samples were simultaneously collected at each station. CTD data were processed according to routines described by UNESCO (1991). Salinity and density was calculated based on the equation of state for seawater (EOS80), with  $\sigma_t = \rho(s, t, 0) - 1000 \text{ kg m}^{-3}$ .

### **Simulations and analysis**

#### *Numerical model simulations*

Regional Ocean Modeling Sys0 (ROMS) is a

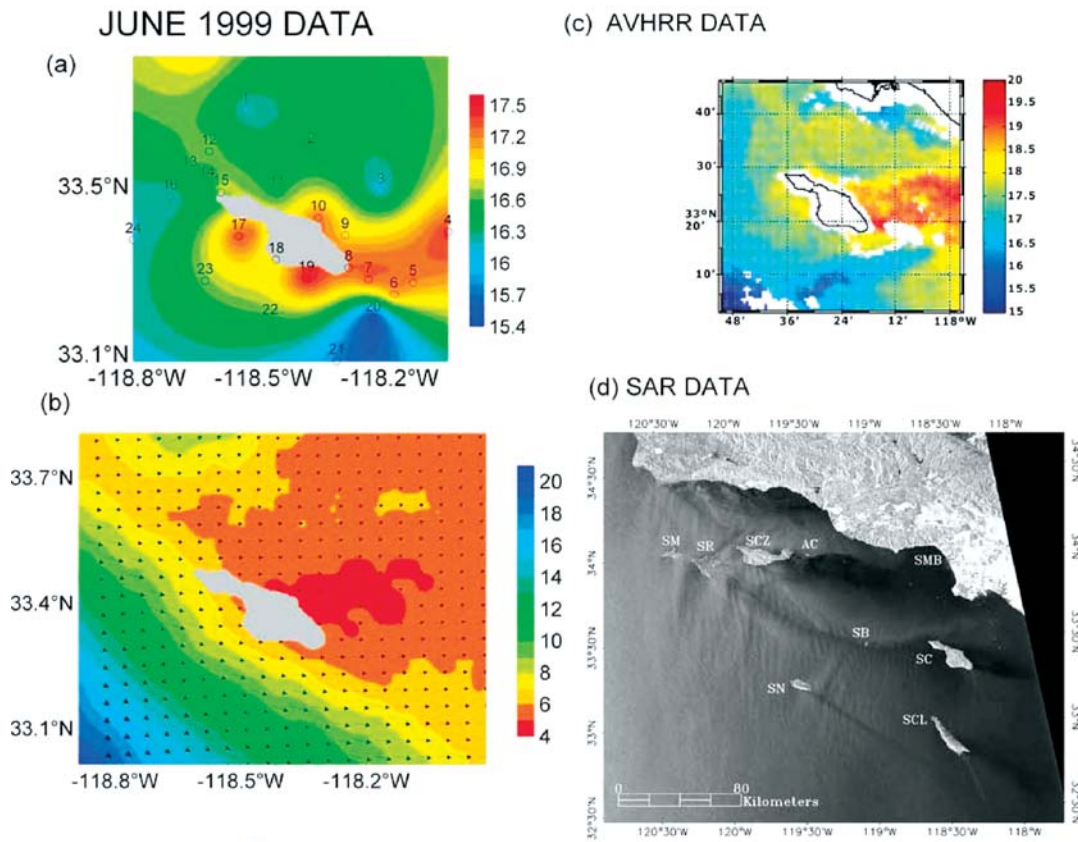


**Figure 3.** In situ data for June 1999 Temperature (a); Ekman depths (DE) and wind fields from COAMPS (b); AVHRR data for the same period showing warmer SST leeward of Santa Catalina Island (c); RADARSAT ScanSAR image from June 8, 1999 at 02:00 UTC of the entire Southern California Bight (d).

free-surface, primitive-equation, curvilinear-coordinate oceanic model in which barotropic and baroclinic momentum equations are resolved separately. The model is written for multi-threaded computer architectures and features high-order numerical schemes for space and time differencing, to optimize the effective resolution of the model. In addition, open boundary conditions in ROMS permit well-behaved, long-term solutions for coastal configurations with open boundaries on three sides, through which the influences of the large scale, external circulation must be conveyed. Detailed description and validation of the model for the west coast of the United States is given in Shchepetkin and McWilliams (1998, 2003, 2005) and Marchesiello *et al.* (2003).

The local, small-scale dynamics in the SCB is studied using embedded domains. The method for embedded gridding takes advantage of the Adaptive Grid Refinement in Fortran (AGRIF) package (Blayo and Debreu 1999), which has the ability to manage an arbitrary number of embedded levels. ROMS nesting procedure is described and validated for the United States West Coast (USWC; Penven *et al.*

2003). Three levels of resolution have been defined: the first level is a 20-km grid USWC domain (forced at the open boundaries by Levitus data, using mixed active-passive boundary conditions as given by Marchesiello *et al.* (2001); parent of a second level which is a 6-km grid subdomain of the whole SCB, which in turn is the parent of the third level, a 2 km-grid subdomain of SMB including Santa Catalina and San Clemente Islands.

Using as forcing monthly climatology extracted from COAMPS wind data, we conducted a multi-year simulation in one-way nesting mode until the solution reached equilibrium. The solution for one year is qualitatively comparable at the different levels, but the magnitude of the current increases with finer resolutions. Moreover, the finest level shows small-scale processes not present in the parent levels.

ROMS solutions are used to illustrate the diversity of currents wake scenarios that might occur around Santa Catalina Island. Seasonal means of Sea Surface Height (SSH) are also calculated to enhance the discussion on seasonality of oceanic conditions around the island.

### *Time-series analysis of low-resolution AVHRR-SST and SeaWiFS chlorophyll data*

We analyzed the persistent signatures of these island wakes using Pathfinder AVHRR data to quantify temporal differences in SST. The data was processed within the scope of NOAA/NASA AVHRR Oceans Pathfinder Project at the Jet Propulsion Laboratory. The SST data were derived from AVHRR using an enhanced nonlinear algorithm (Walton 1988). We used daily data for the descending pass (night-time) on global equal-angle grids of 4096 pixels/360° (~9.28-km resolution). Only the “best SST” data (i.e., highest quality pixel values) were considered. Interim versions V4.1 (2000-2001) and V4.1 (1997-1999) were used to derive absolute SST values for the time-series analysis.

The remotely-sensed data collected by SeaWiFS used in this study were obtained from NASA Goddard Space Flight Center, Distributive Active Archive Center (GSFC DAAC) (Acker *et al.* 2002). The data we used allowed for the time-series analysis of sea surface chlorophyll concentration from different sides and at different distances from the islands and we used daily Level-3 SMI (Standard Mapped Images) data of SeaWiFS surface chlorophyll calculated during reprocessing 4 (Version 4). Level 3 SMI SeaWiFS chlorophyll data were interpolated to a regular grid of equidistant cylindrical projection of 360°/4096 pixels (~9.28 km) resolution (similar to Pathfinder SST). Understanding that the values of sea surface chlorophyll concentration derived from satellite measurements are subject to significant inaccuracy due to technical problems with remote-sensed observations, therefore we did not attempt to compare the remote-sensed data to *in situ* chlorophyll absolute values. Instead, we use the remotely-sensed observations for qualitative analysis of the cycles of phytoplankton development around the islands. Accordingly, we use the terms “remotely-sensed surface chlorophyll concentration”, “chlorophyll biomass,” and “phytoplankton biomass” synonymously, taking into account the correlation between remotely-sensed surface pigment concentration and total pigment concentration in water columns (Smith and Baker 1978) and the good correlation between satellite and *in situ* chlorophyll observations off California (Chavez 1995).

We calculated mean values within the grids of different size “quadrants” centered on each island. The smallest quadrants were 2x2 pixels, i.e., about 19x19 km, for San Nicolas and San Clemente

Islands; for Santa Catalina Island, due to its shape and orientation within the SCB, the size of the quadrants was 3 (horizontal) by 2 (vertical) pixels. Then mean chlorophyll values were estimated for quadrants of 4x4, 6x6, and 8x8 pixels; for Santa Catalina Island, values were estimated for quadrants of 4x6, 6x8, and 8x10 pixels. The largest quadrant for each island was treated as the “background” chlorophyll concentration in the waters surrounding the island. The change in ratio between chlorophyll concentration in smaller quadrants and the background concentration (largest quadrant covering the whole island) was analyzed as a measure of the island mass effect. For example, if averaged monthly values for a particular quadrant were below 0, the quadrant was consistently colder or less productive than its regional counterpart; whereas if monthly values were above 0, the quadrant was warmer or more productive than its regional counterpart. We also used the averaged monthly data from the regional quadrants to determine the seasonality of productivity around the islands.

## Results

### Wind-induced wakes

We have assembled for the 11 - 13 June, 1999, cruise a mosaic of coincidental data collected *in situ* and from AVHRR and SAR satellite sensors (Figures 3a - 3d). Surface temperature as measured by the CTD (Figure 3a) showed higher gradients mostly to the southeast of Santa Catalina Island with temperatures varying from 17.2 to 17.5°C. This was also apparent in the wind and Ekman depth ( $D_E$ ) patterns (Figure 3b). Winds were generally weaker leeward of the island than they were windward, hence the calculated  $D_E$  varied between 4 m within the sheltered (leeward) region to up to 20 m on the exposed (windward) region. Satellite AVHRR data for June 13, 1999 (22:56 GMT), also showed a patch of warm SST leeward of Santa Catalina Island (Figure 3c). Temperature in the warm patch varied between 18.5 to 20°C, whereas in the other areas SSTs only reached a maximum of 17°C. Differences between *in situ* and satellite SST values can be due to the fact that our *in situ* measurements were collected over a three-day period (from June 11 - 13, 1999), whereas satellite data is a single observation in space and time. Furthermore, Multi-Channel Sea Surface Temperature (MCSST) algorithms also suffer from

unaccounted processing inaccuracies (Robinson 2004). In any case, SST gradients for both platforms (*in situ* and remote sensing) show similar patterns, with warm water to the south of Santa Catalina Island representative of the wind leeward wake. RADARSAT ScanSAR imagery obtained on June 8, 1999, shows that there was a strong wind wake southeast of Santa Catalina Island, as revealed by a dark patch (i.e., zone of low backscatter) indicative of reduced sea-surface roughness. The SR wind wake appeared to reach all the way to SC; the SCZ wind wake reached SMB; the SN wind wake running ~50km to the southeast; and the SC and SCL wind wakes were also clearly visible (Copyright Canadian Space Agency 1999; Figure 3). In fact, this image reveals wind wakes had formed leeward of most of the islands in the SCB. The low backscatter signal from the SAR image extends to 50 km offshore of Santa Catalina Island and ~100 km offshore of Santa Cruz Island, sheltering part of the Santa Monica Bay (SMB; Figure 3d). Also readily apparent in this image are the concurrent sea-surface

manifestations of atmospheric lee waves, particularly southeast of Santa Rosa Island.

As previously proposed by Caldeira and Marchesiello (2002), these inshore sea surface warm signatures are probably a result of solar heating and weaker winds in the SCB. Heat advection from southern tropical waters is the traditional explanation for the high SST often observed in inshore regions of the SCB (Hickey 1979). Nevertheless, solar heating and weaker winds may also play an important role in the build-up of these lateral (inshore-offshore) SST gradients for the whole SCB (Caldeira and Marchesiello 2002).

In order to analyze the vertical structure of wind-induced wakes, we selected CTD stations from our June 1999 cruise of exposed and sheltered regions around Santa Catalina Island. There are three types of thermoclines: permanent, seasonal, and shallow thermoclines (Figure 4). The plots in figure 4 represent various scales of depth and temperature in order to emphasize the different scale thermal gradients. That is, shallow, seasonal and permanent thermo-

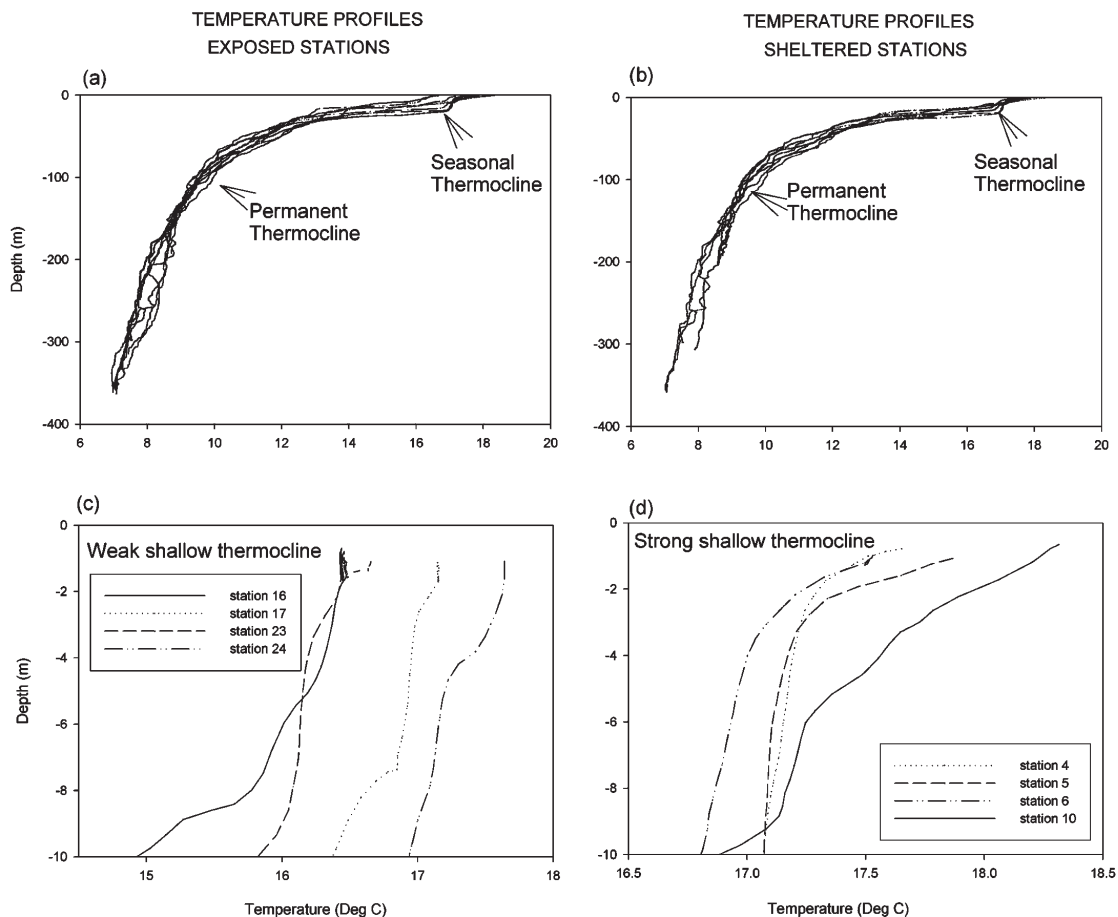
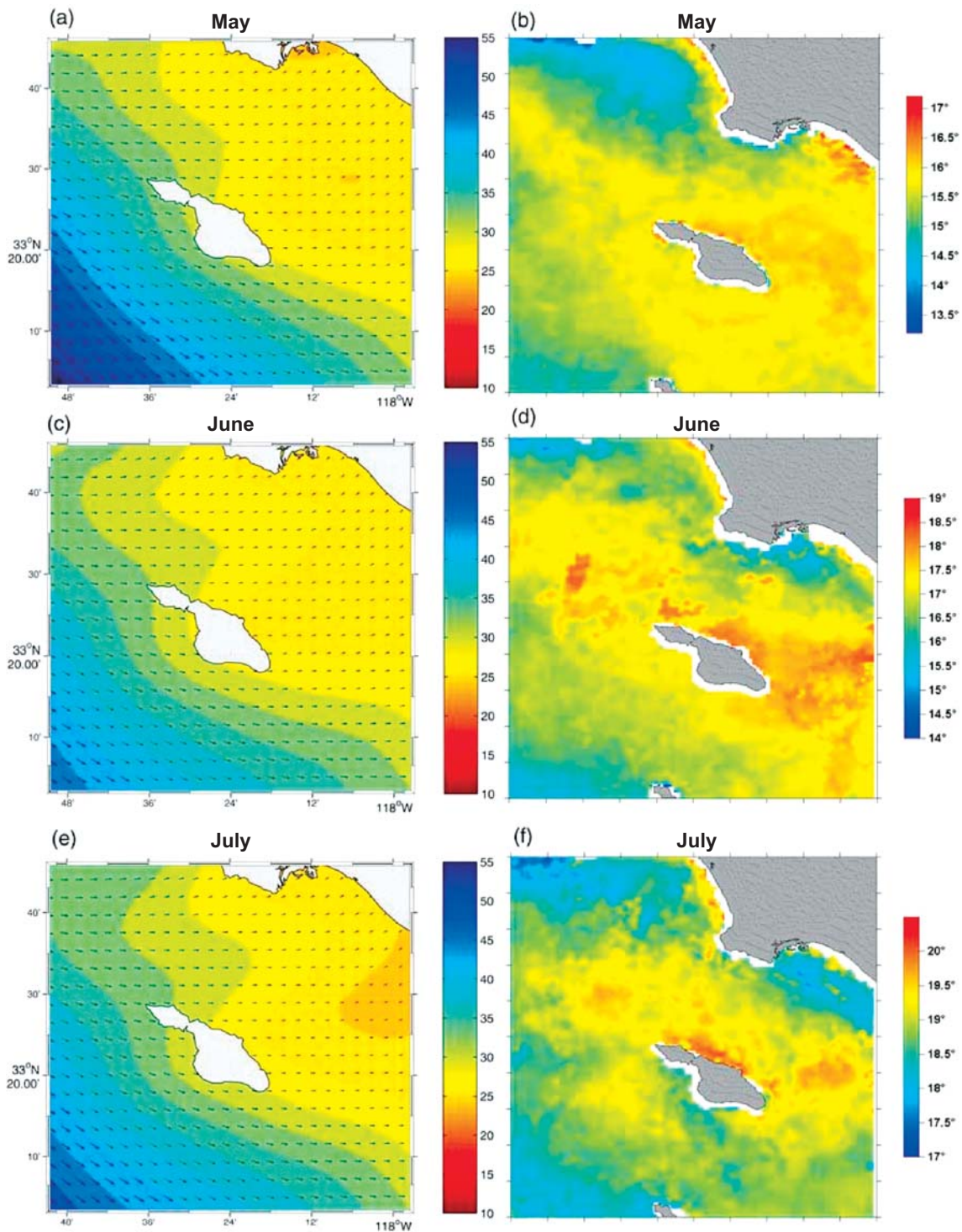


Figure 4. Temperature profiles in exposed (a and c) and sheltered stations (b and d).



**Figure 5. Average wind and SST conditions for the period of May to July (1998 - 2000 data). Left plots represent wind conditions and Ekman depths ( $D_E$ ), color scale in meters; and right plots represent SST, color scale in degrees Celsius.**

clines. Stations 4, 5, 6, and 10 (see Figure 3 for station locations) were on the leeward (sheltered) side of Santa Catalina Island, whereas stations 16, 17, 23, and 24 were on the windward (exposed) side. A better defined shallow thermocline is observed in the shel-

tered stations compared with weak shallow stratification on the exposed stations. It is evident that shallow thermoclines had a deeper signature (4 m) at the sheltered stations (stations 4, 5, 6, and 10) than at the exposed stations (2 m; stations 16, 17, 23, and 24).

In order to evaluate the daily persistence of this wind-induced wake event, around SC, we have taken two-year (1998 - 2000) wind (COAMPS) and AVHRR SST datasets and calculated monthly averages (Figure 5). We elected to present only the three representative (spring and summer) months out of the twelve-month series because that is when the wind wakes were most prominent. The results, shown in Figure 5, revealed that the wind-induced wake signature is present during both spring and summer months sampled. This figure shows the wind-sheltering effects off the southeast end of SC. Winds are also generally stronger during spring and summer. Stronger winds caused stronger gradients on the  $D_E$ , suggesting weaker wind mixing. Weaker mixing allows for higher heat storage and warmth of the SST ( $17^\circ\text{C} - 20^\circ\text{C}$ ) leeward of the island (left plots). The  $D_E$  varied from 25 - 28 m in the sheltered

regions to 50 - 55 m in the exposed regions. The SST gradients reach  $2^\circ\text{C} - 3^\circ\text{C}$  difference between sheltered and exposed regions around SC.

## Current-induced wake

### *In situ data*

A mosaic data from the November 16 - 20, 2001 cruise reveals a nucleus of cold water ( $17.4^\circ\text{C}$ ) at the surface, northwest of Santa Catalina Island (Figure 6a). High-density water ( $24.36 \text{ kg m}^{-3}$ ) was also detected in the same general area (Figure 6c). Coincidental SST from AVHRR (November 19, 2001) showed a tongue of  $17^\circ\text{C}$  in the same region (Figure 6d). A RADARSAT SAR image (Figure 6e) acquired within this same period of time (i.e., November 16, 2001) indicates the presence of an eddy feature, to the northwest of Santa Catalina Island. Other features were present off the southeast

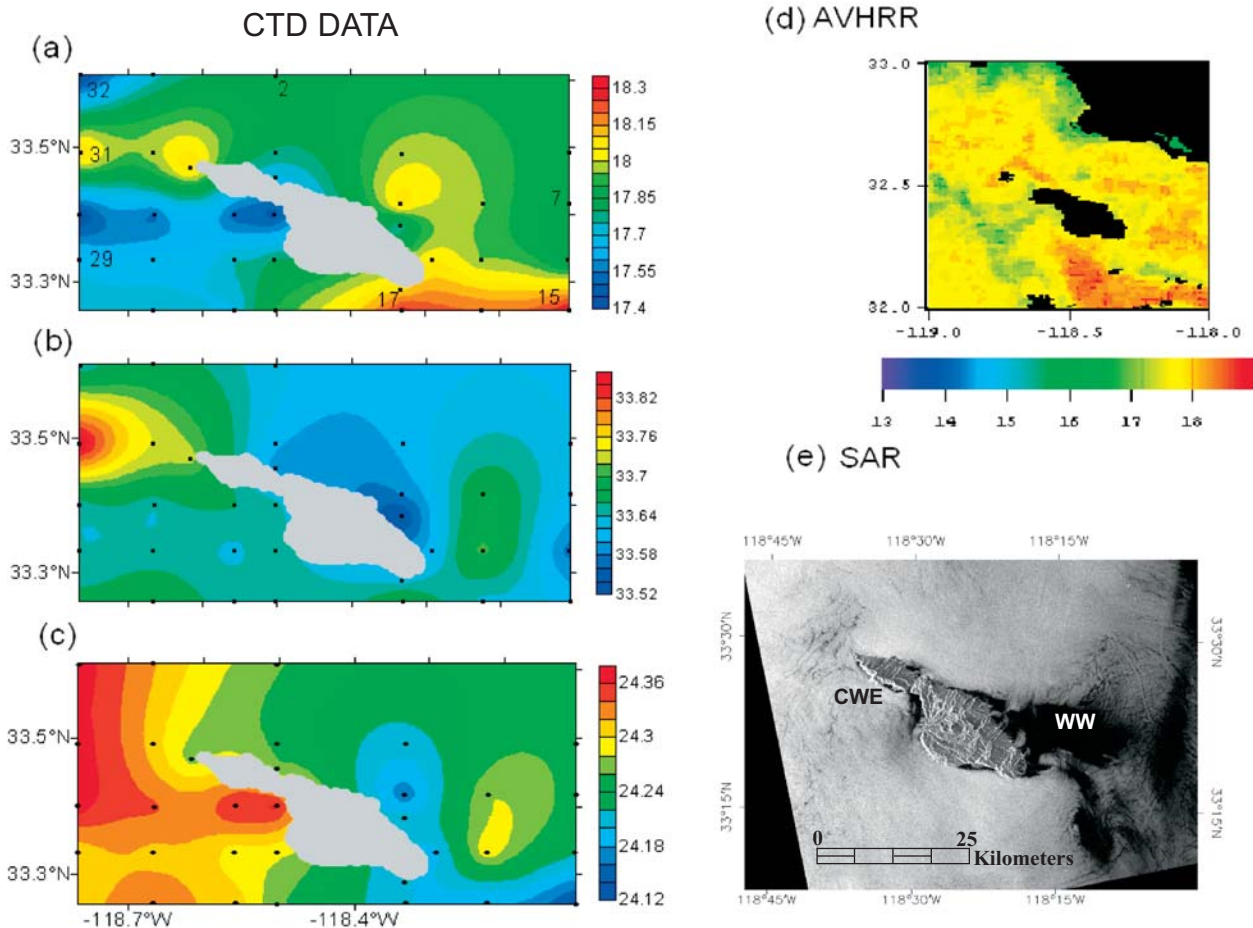


Figure 6. Left side: data for the November 16-20, 2001 cruise - temperature in  $^\circ\text{C}$  (a); salinity in ppt (b); and  $\sigma_t \text{ kg m}^{-3}$  (c). The data show a tongue of cold water to the northwest side of the island. Salinity and density was higher to the north as well. Right side: AVHRR November 19, 2001, 10:38 UTC (d) and RADARSAT SAR image from November 16, 2001 at 01:42 UTC (e). Interesting features are evident to the northwest of Catalina (e), including surface slicks potentially indicative of an eddy or other surface circulation feature, and the same area seen by AVHRR (d) is somewhat colder ( $1^\circ\text{C}$ ) than its surroundings.

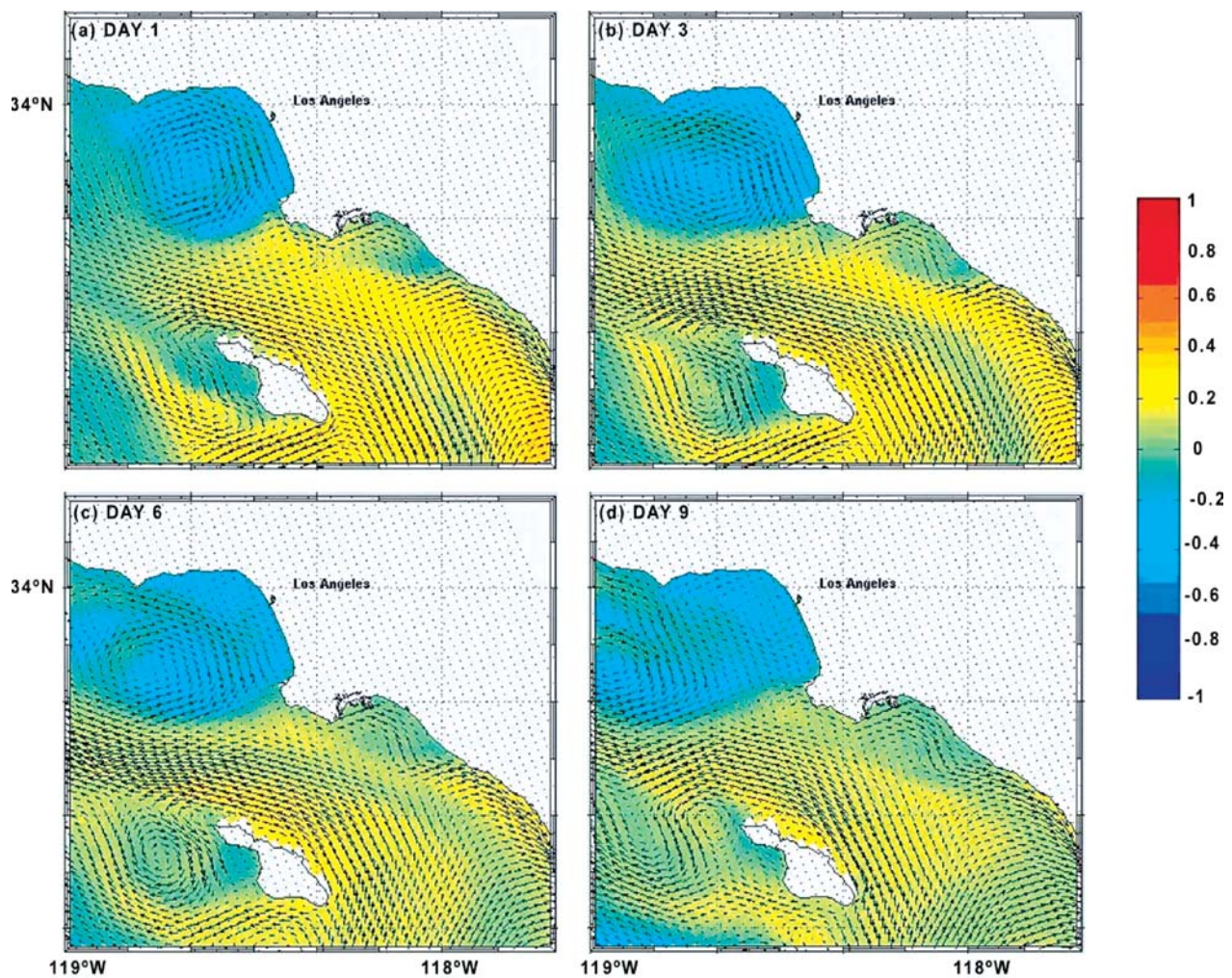


Figure 7. Snapshots from ROMS 1-year simulation showing the progressive (9-day) formation of a northwest island wake with the eddy advecting away from the island after 9 days. The eddy was anticyclonic and reached 30 km in diameter. Color bars represent SST anomalies.

end of the island, including a low wind zone and more surface slicks.

### *Numerical simulation study*

The formation of a northwest wake, as observed during our November 2001, cruise is well illustrated by ROMS simulations (Figures 7a - 7d). Four snapshots, three days apart, show an anticyclonic eddy being formed on the west side of Santa Catalina Island (Figure 7a), requiring a total of nine days from birth to detachment (Figure 7d). The eddy reached 30 km in diameter and transported cold water in its core. The angle of the jet affecting Santa Catalina Island at the time of our cruise was normal to the island shelf. However, due to the asymmetric shape of the island, slightly bulging to the west, the island offers unequal resistance to the incoming current.

To assess the occurrence of this and other wake

scenarios we analyzed one-year ROMS solutions, after the model reached equilibrium (Figure 8). Six different scenarios were distinguished using ROMS solutions. The percentages indicate how often each scenario occurred within the 121 yearly frames analyzed (every three days). The six patterns of flow are: West island wake, 35%; Northeast eddy, 32%; North Von Karman Street with upwelling of cold water, 20%; Northwest eddy, 6.5%; Dipole eddies to the northwest and northeast of the island, 4%; and Southeast eddy, 2.5%.

There were also various combinations of these six scenarios. For example, the northwest wake scenario often evolved into Von Karman Streets and/or northwest eddies. After a brief period of time (9 to 12 days), fully-formed eddies spun from the north side of the island. Another example of the complexity of flow regimes is illustrated by Figure 8f. This

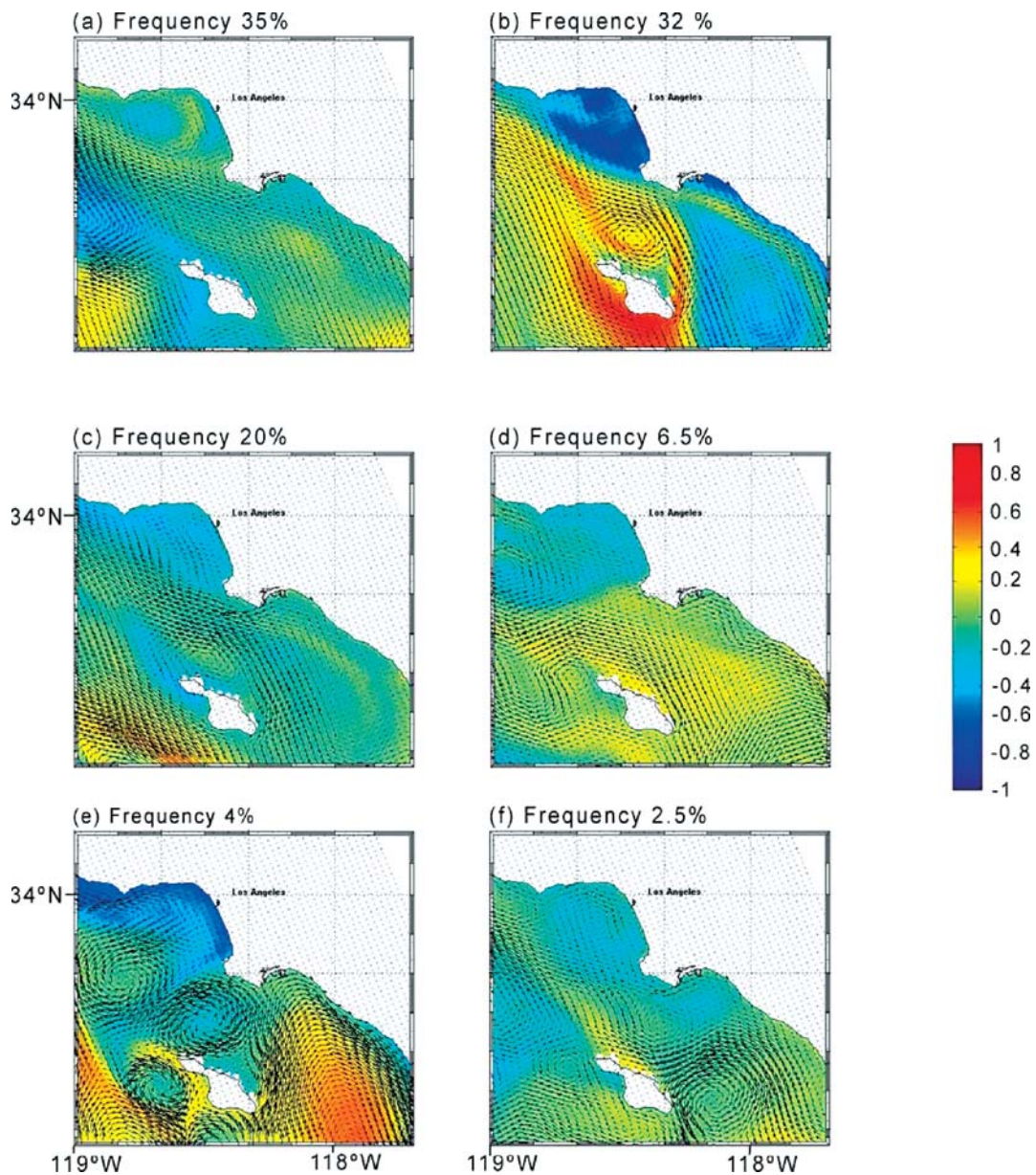


**Figure 8. Current island wakes scenarios resolved by ROMS during the 1-year simulation ordered from most abundant to less abundant: west wake(a); northeast eddy (b); north Von Karman Street with upwelling of cold water (c); northwest eddy (d); dipole eddies to the north of the island (e); and southeast eddy (f).**

snapshot shows a cyclonic eddy forming to the southeast of the island; however, there are also anti-cyclonic and cyclonic eddies forming to the northeast and to the west of the island. We do not contend with these examples that we have fully evaluated the dynamics of the surface ocean currents around Santa Catalina Island. However, we do wish to illustrate that a classical approach, which averages long-term geostrophic conditions, will not take into consideration all the island wakes scenarios compiled herein (Figure 8).

In terms of the temporal variability in ROMS simulations we found that current wakes are often formed to the north of Santa Catalina Island during winter and summer (Figures 9a and 9c) and to the south/southeast during spring and fall (Figures 9b and 9d). Figure 9 shows contours of Sea Surface Height (SSH) derived from the ROMS solutions discussed above. Each panel represents the average conditions for a season. Sea Surface Height is a good measurement of the island wake activity since island generated eddies, fronts and upwelling sys-

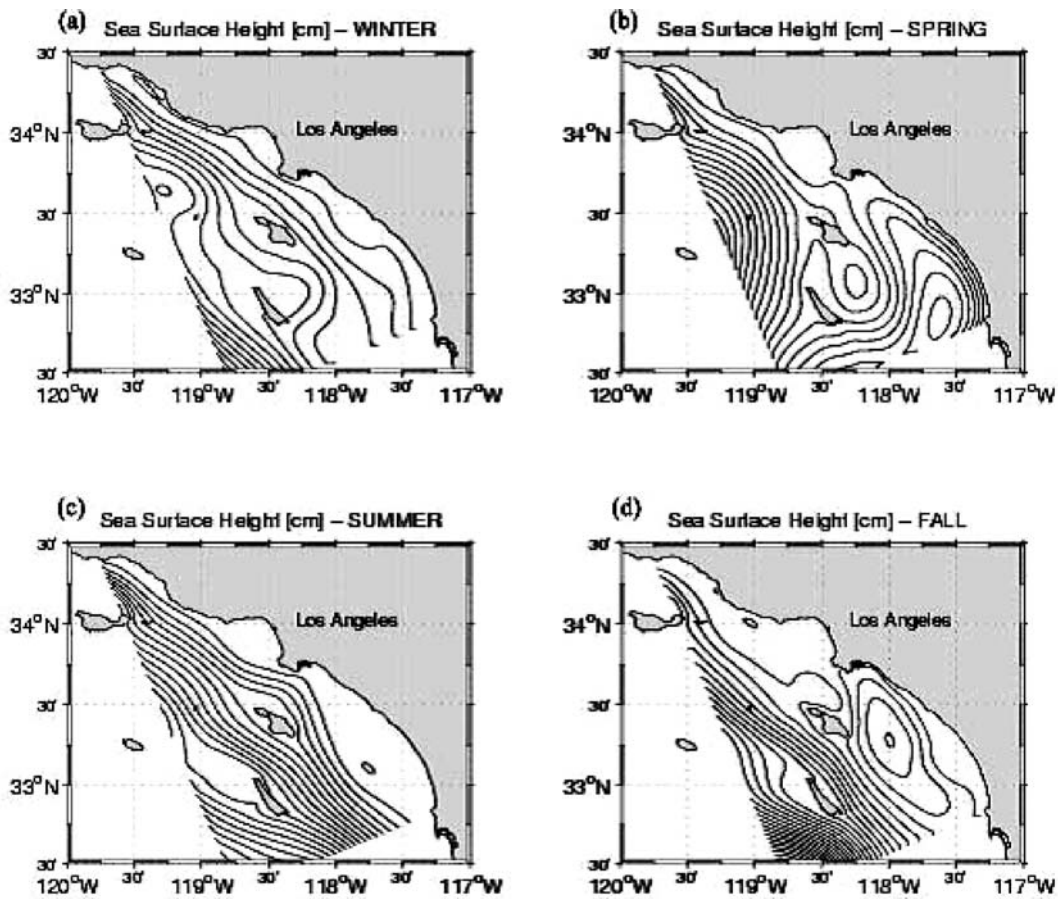


**Figure 9. Sea Surface Height analysis for the Southern California Bight from level 3 (2 km) embedded domain. Units are in cm, and the contour interval is 0.5 cm.**

tems promote convergent and divergent circulation cells with a SSH signature. We present ROMS SSH scenarios as probable seasonal average conditions for the SCB. The north during winter and summer (Figures 9a and 9c) and south during spring and fall (Figures 9b and 9d) current wake patterns reflect well the seasonality of the wind stress patterns in the SCB. Figure 9 also shows a wake signature, even in the mean seasonal fields. The strongest wakes occur in summer when the poleward California Counter Current is also the strongest. Winter and summer showed wakes to the north of Catalina Island whereas spring and fall have shown wakes to the south. These are seasonal averages but only for a three-year period, therefore the seasonal means still have mesoscale features included.

### *Submesoscale dynamics in the SCB*

Some of the interesting submesoscale dynamics that take place around Santa Catalina Island were described recently by DiGiacomo and Holt (2001). On the basis of SAR imagery acquired between 1992

to 1998, approximately half of the SCB submesoscale eddy activity they observed occurred around Santa Catalina Island (Figure 10). However, the majority of these (~66%) were submesoscale eddies of 1 - 10 km in diameter, whereas in our ROMS solutions the diameter of most eddies varied between 10 and 30 km. There are also more anticyclonic features in the ROMS solutions than were observed by the SAR imagery.

### **Wakes off other islands in the Southern California Bight**

#### *Wind wakes*

Wind and current wakes are not unique to Santa Catalina Island but occur off most islands of the SCB. In fact, we hypothesize that current wakes contribute to a significant part of the submesoscale dynamics of the SCB and therefore to the input of nutrients to the euphotic zone. All islands of the SCB produce some manner of wind wakes as illustrated above (Figure 3d). On this occasion the Santa

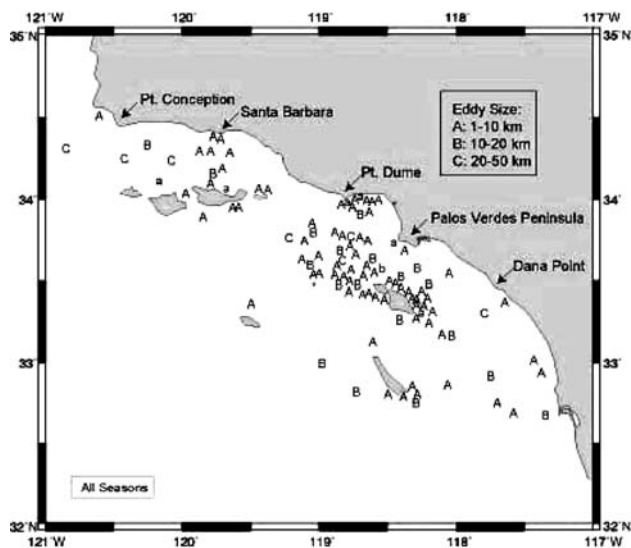


**Figure 10.** Total distribution map of eddies detected in the Southern California Bight via ERS-1 and ERS-2 SAR images from 1992 to 1998. Size of eddies indicated by the following: 1 - 10km (A); 10 - 20km (B); 20 km and greater. Capital letters indicate cyclonic eddies (C), and lowercase letters indicate anticyclonic eddies (a and b).

Rosa Island (SR) wind wake, reaches Santa Barbara Island (SB); the Santa Cruz Island (SCZ) wind wake reaches SMB; the San Nicholas Island (SN) wind wake runs 50 km south, approximately eight times the diameter of the island; the Santa Catalina Island (SC) and San Clemente Island (SCL) wind wakes can be distinguished also. We have identified numerous ERS-1/2 and RADARSAT SAR images that show concurrent incidences of wind wakes off multiple SCB islands. As such, SCB island wind wake effects should not necessarily be considered independently in future surveys. For example, the SR wind wake shown in Figure 3d reaches as far as SC and impacts the local sheltering effects of that island. Another aspect that was clear from our review of these SAR images was that offshore islands, although smaller, showed longer leeward streets as a result of stronger offshore winds.

#### *Current wake off San Clemente Island*

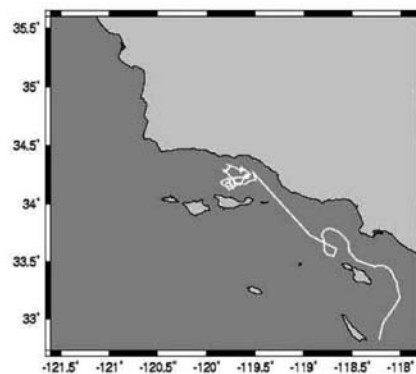
ERS-1/2 SAR imagery (during the two missions so-called “tandem phase”) from January 26, 1996 (not shown) and January 27, 1996 (Figure 11b), 1996, revealed a current eddy southeast of San Clemente Island that was approximately 18 km in diameter. It had an apparent translational speed of 9  $\text{cm s}^{-1}$  and it tracked east-southeast over the course

of two days. Near-coincident drifter releases from the Santa Barbara Channel-Santa Maria Basin Coastal Circulation Study revealed that flow during this time was indeed equatorward (Figure 11a), supporting the above interpretation of the equatorward forcing of this eddy. These San Clemente wake eddies are often observed in our extensive ERS-1/2 and RADARSAT SAR archive and deserve further investigation.

#### **Time-series analysis and the island mass effect phenomenon**

The cumulative remotely-sensed surface chlorophyll concentration for the SCB (Figure 12) reflects the climatology of both productivity and hydrology of the region. The highest concentration, compared to the (1-1.5  $\text{mg m}^{-3}$ ) around the islands, was detected near the continental shelf ( $\sim 3 \text{ mg m}^{-3}$ ) and at the upwelling region of PC. The exception is a rich patch of chlorophyll concentration developed north-

(a)



(b)

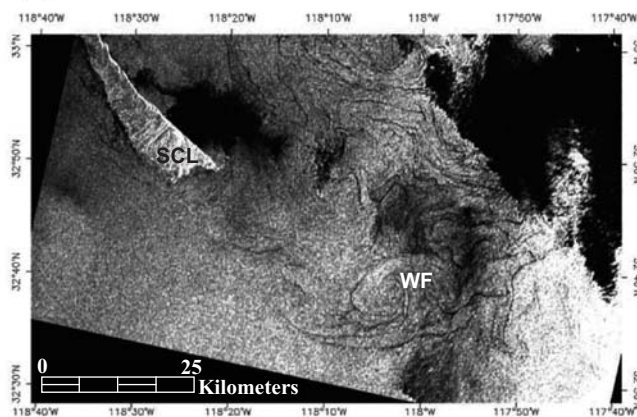


**Figure 11.** Track of drifter was released in the Santa Barbara Channel, north of Santa Cruz Island (a). ERS-2 SAR image of San Clemente Island and vicinity on January 27, 1996, at 18:32 UTC (b). WF denotes wake eddy. SCL denotes San Clemente Island.

west of SB separated from the upwelling enrichment patch of PC. However, time-series variability around SC, SCL, and SSN (square regions in the cumulative distribution map; Figure 12) shows a seasonal pattern around the islands (Figure 13). This suggested the occurrence of nutrient enrichment around islands and the occurrence of the island mass effect.

The effect of SN on surface chlorophyll concentration is most pronounced, especially during summer months (Figure 13a); in July-August, the chlorophyll concentration in the small quadrants is almost twice the background concentration. This effect is also present in the map of cumulative chlorophyll distribution in the SCB (Figure 12). However, the island mass effect of SCL and SC is not as evident (Figures 13b and 13c). In late winter and early spring (January-March) chlorophyll concentration in the small quadrants exceeds background concentration by 10-15%. During mid-spring, significant differences are not typically observed. During late spring and summer (especially in May and August) SC shows a “negative island mass effect”. By negative island mass effect, we mean that the background chlorophyll concentration exceeds the values observed in the small quadrants.

We believe that the negative island mass effect around SC results from its proximity to shore, under the influence of the coastal high

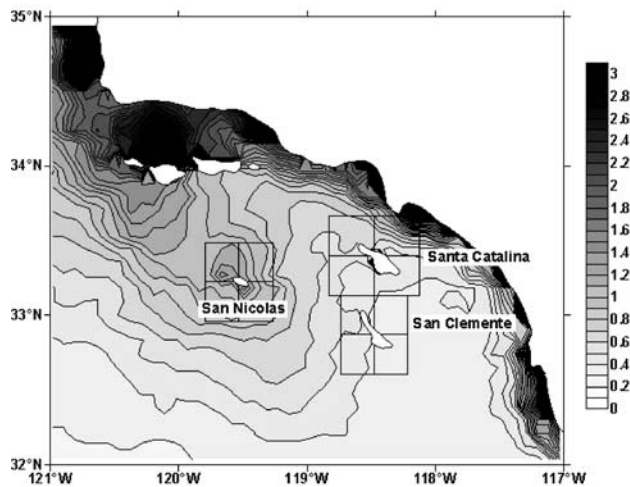


**Figure 12.** The cumulative distribution of surface chlorophyll ( $\text{mg}/\text{m}^3$ ) in the Southern California Bight averaged over the entire period of SeaWiFS observations (September 1997 to July 2002). The rectangles around three islands (San Nicolas, San Clemente, and Santa Catalina) indicate the zones where Level 3 data pixels were averaged for time-series analysis.

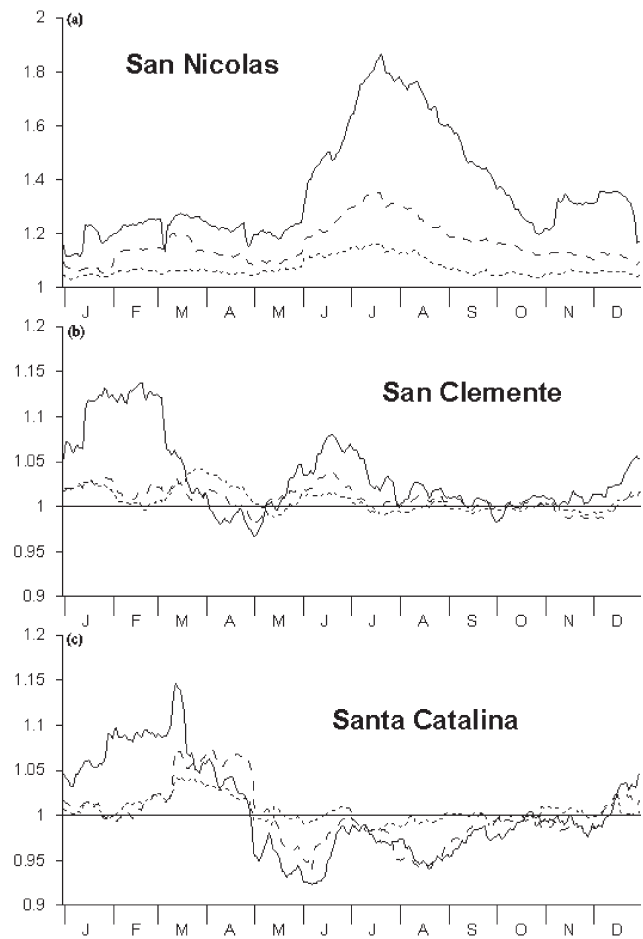


**Figure 13.** Island mass effect of San Nicholas, San Clemente, and Santa Catalina islands on productivity. Seasonal variations of the ratio between SeaWiFS chlorophyll means in the different size quadrants 2x2 (solid line), 4x4 (dashed line), 6x6 (dotted line) and 8x8 pixels.

chlorophyll concentrations; the northern eastern part of the 8x10 rectangle is located within the continental shelf zone, where chlorophyll concentration is always higher than offshore. In general however, the seasonality of the island mass effect for SC and SCL could be related to the seasonality of the CCC. Hickey (1998) showed that poleward flow within the SCB is strongest during winter and summer months. Therefore, we would expect that current wakes and subsequent upwelling of cold nutrient rich waters to be highest during such events; this is also in agreement with our averaged SSH from ROMS numerical solutions.

Looking at the individual island cases increase in sea surface chlorophyll is often concurrent with decrease in SST (Figures 14a - 14c). For SN, we hypothesize that the summer increase

in chlorophyll concentration is related to the inshore shift and increase in the equatorial flow often observed for the CC.

Figures 14a - 14c illustrate the SST anomalies in 3x3 quadrants located to NW, NE, SW, and SE of each island (here we use the term “anomalies” meaning the differences between SST in the 3x3 quadrant and the background SST in 6x6 quadrant surrounding the entire island).

The remote-sensed surface chlorophyll concentration to the NW of SN is permanently higher (Figure 14a), resulting from general gradient of chlorophyll concentration in SCB (Figure 12). The CC transports cold water rich in chlorophyll from NW along SN. At the same time, chlorophyll heterogeneity directed to the NE, SW, and SE of SN exhibits seasonal variations.

In late winter (February-March) positive chlorophyll gradient is directed to the NE, then

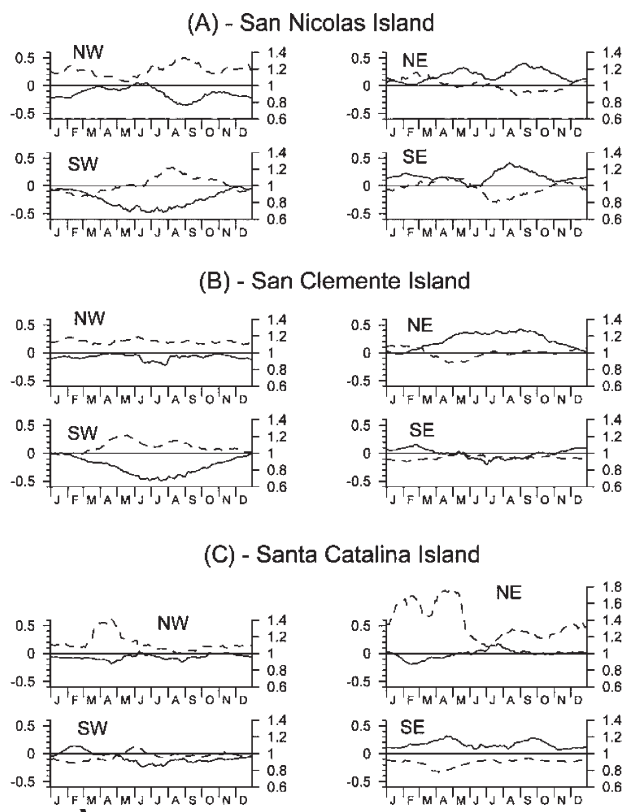


**Figure 14.** Difference between sea surface temperature and derived chlorophyll, in 3x3 quadrants located in four directions around the Islands and 6x6 background values surrounding the islands: San Nicolas Island (A); San Clemente Island (B); Santa Catalina Island(C). Data shows decrease in SST (solid line) generally concurrent with increase in sea surface chlorophyll (dashed line).

(April-May) it shifts to the SE, and later (starting from July) it is directed to the SW, when the equatorward effect of the CC is supposedly greater. The regularities of spatial heterogeneity in chlorophyll, resulting from seasonal variations of circulation patterns, are also evident on SCL (Figure 14b). To the NW of the island chlorophyll concentration is permanently higher.

In winter, chlorophyll is higher to the NE whereas in summer and autumn it is higher to the SW of the island. SCL island is located closer to the shore than SN. In summer, the strengthening of the CCC, which transports low chlorophyll water poleward, enhances the cross-shelf chlorophyll gradient. Chlorophyll distribution around SC island (Figure 14c) manifests two features: high chlorophyll concentration to the NE during winter-spring, and to the NW during spring. Higher chlorophyll concentrations to the NW of SC in spring can be explained by CC migrating onshore, weakening of the CCC.

## DISCUSSION

Several conclusions can be drawn from this first study of island wakes in the SCB. Wind induced island wakes must be distinguished from current induced wakes. Santa Catalina Island, given that the predominant ocean currents flow opposite to the predominant wind conditions, offers a unique opportunity to explore the relative contribution of the two types of wakes on the transport and retention of biogenic materials. The central mountain range on Santa Catalina Island offers resistance to the predominant incoming north-east winds, sheltering the leeward side of the island. Weaker wind in the lee induces weaker mixing and surface waters store more heat from the incident solar radiation (Caldeira and Marchesiello 2002, Robinson 2004). The CCC moving poleward is disrupted by the bathymetry of the island, with formation of a current island wake to the north side of Santa Catalina Island. Current and wind wakes occur on opposite sides of the island due to differences in the direction of the predominant wind and surface currents. This study is the first of its kind to feature reported data for opposite sides of an island. Most surface currents are wind driven and therefore wind; therefore, current directions are mostly parallel. Wind and current wakes around Santa Catalina Island may also occur concurrently, particularly during strong equatorial push and/or Santa Ana wind events.

## Wind-induced wakes

In their review of small scale eddies of the SCB using SAR and AVHRR data, DiGiacomo and Holt (2001) has also detected features with warm and cold surface signatures between the southeast side of Santa Catalina Island and the coast (Palos Verdes Peninsula). Prior to that, Owen (1980) reported eddy-like patterns in drogue tracks on the wind wake side of Santa Catalina Island. The contribution of wind-induced eddies to the production of both cyclonic and anticyclonic eddies requires further investigation in the SCB before conclusions can be drawn. Further, shallow thermoclines can be considered analogous to the previously defined “atmospheric mixed layers” (Imberger 1985). Calm conditions, often felt in the morning, can lead to daily heating of the surface layer. Afternoon sea breezes can deepen the surface layer, and night cooling can remove heat accumulation. This should be a theme for further investigation in the SCB. Time-series analysis of diurnal thermoclines could give us further insights on the mechanisms that contribute to warming and cooling of the inshore surface waters. Wind and current wakes are also generated by other islands of the SCB and their relative importance and interaction require further attention. Future work should consider the use of integrated multi-sensor (e.g., ocean color, SAR, SST) approaches, using single (e.g., ENVISAT) or multiple platforms, to identify small-scale island-generated features in the SCB and elsewhere.

Daytime heating in the absence of strong wind mixing, for the Canaries Archipelago also led to the formation of a warm, stratified layer at the surface. In exposed regions, strong wind-induced mixing masks the effect of surface heating to produce a uniform surface layer (Barton *et al.* 1998). The crucial difference here is that these wind wake effects for Santa Catalina Island seem to be associated with gradients in much shallower water (2 - 4 m); whereas in the Canaries these wind wakes were attributed to wind curl effects with much deeper signatures.

According to Bray *et al.* (1999), wind stress curl is stronger ( $4 \mu\text{Pa/m}$ ) between the channel islands and PC all-year round when compared to the rest of the Bight ( $<1 \mu\text{Pa/m}$ ). As shown by Bray *et al.* (1999), the highest stress curl occurs between Santa Rosa and Santa Catalina Islands, sometimes reaching San Clemente Island (highest for spring and summer). Therefore, future studies might also want to

consider the relative contribution of each island to the overall sheltering effect of the inshore waters.

## Current-induced wakes

### *Reynolds number theory*

Current-induced island wakes is a classic fluid dynamics problem (Barkley 1972; Coutis and Middleton 1999; Dietrich *et al.* 1996; Furukawa and Wolanski 1998; Wolanski *et al.* 1984, 1996). The simplest two-dimensional approach, considering incident laminar flow, is to predict the formation of wake types, i.e., from attached eddies to fully turbulent Von Karman Vortex Streets, on the basis of the Reynolds number ( $R_e$ ) theory:  $R_e = UL/A_h$ , where  $U$  is the incident current speed;  $L$  the width of the island and  $A_h$  the horizontal Austausch coefficient, which is a measure of the horizontal eddy diffusivity. At very low  $R_e$  ( $R_e < 0.5$ ), flow around obstacles is controlled by friction occurring entirely within the frictional boundary layer, and it is laminar and symmetric. At slightly larger Reynolds numbers ( $2 < R_e < 30$ ) the boundary layer separates behind the obstacle, creating a vortex pair with opposite rotation and central return flow. Moderately high  $R_e$  ( $40 < R_e < 70$ ) leads to the formation of a wake, which exhibits wave disturbances or instabilities at its interface with the undisturbed current. Very high  $R_e$  ( $80 < R_e < 90$ ) produces the separation of the vortices from the obstacle. Vortices separate in turn from either side and drift away with a velocity of  $0.8U$ , forming a downstream sequence of vortices with alternate sense of rotation, the so-called Von Karman Vortex Street (Tomczak and Godfrey 1994). Eddies are intense energy dissipaters and island current wakes are regions of high-energy dissipation. The  $R_e$  value derived to characterize the different wake types was determined by towing an object through a tank with fluid at rest. In the ocean, however, the currents are moved by winds, internal pressure gradients, or tides. There are also important distinctions that should be made between island wakes in deep water and those made in shallow water (Wolanski *et al.* 1984; Tomczak 1998; Wolanski *et al.* 1984). However, given that our  $D_E$  is much less than the ocean surrounding water depth, Santa Catalina Island should induce deep-ocean type current wakes. Therefore, for an average speed of CCC of  $0.3 \text{ ms}^{-1}$  (CalCOFI data), considering an average  $A_h$  value of  $100 \text{ m}^2 \text{ s}^{-1}$  (Aristegui *et al.* 1994; Tomczak, 1998), the  $Re$  for Santa Catalina Island is

58, which predicts a wake formation with wave disturbances but not as fully turbulent as a Von Karman Vortex Street (ROMS scenario c discussed earlier; Figure 7c). However, it is important to note that Santa Catalina Island shelf is not a cylinder, such as are the model islands used in laboratory simulations. This shelf is ridge-like in shape, and therefore a three-dimensional numerical model, such as ROMS, would better represent the dynamics of the flow.

### *Numerical simulation study*

Eddies that spun off the shelf of Santa Catalina Island in ROMS simulation often reached SMB and other coastal areas. Conversely, eddies being formed within the SMB sometimes reached the Channel Islands. Due to the complex nature of the surface currents in this region, we suggest that equatorial flow might also occur during other periods around Santa Catalina Island. Bray *et al.* (1999), for example, suggests that the equatorial flow in the SCB might be a result of coastal upwelling. However, equatorward traveling geostrophic eddies (30 - 60 km, well within the 100-km Rossby radii), as shown in our simulations, also cause an equatorward transport at the surface, between Palos Verdes and Santa Catalina Island.

Our simulations highlight geostrophically balanced flow, off Southern California, divided by the Santa Rosa Ridge; with poleward flow within the SCB and equatorward flow offshore. The exception occurs in spring when the equatorward anomaly weakens or reverses the poleward flow in the Bight (as previously emphasized by Hickey (1992, 1993, 1998). In contrast, in our numerical solutions for flow on each side of Santa Catalina Island, opposing flows were often observed. For example, San Pedro Basin regularly exhibited surface flows traveling in the opposite direction to flows in the Santa Catalina Basin, between San Clemente and Santa Catalina Islands (also shown by drifter data discussed below).

ROMS simulations suggest that a small change in the angle of attack of the incoming current can dramatically change the nature of the island current wakes. For example, scenario b in Figure 8 was induced by a strong jet reaching the island, at a 45° angle from the west, whereas scenario a was induced by the convergence of opposing currents to the west of Santa Catalina Island.

The resident time of eddies and wakes, formed around islands are of great importance when considering their biological effects (Hamner and

Hauri 1981a, b; Wolanski *et al.* 1984; Wolanski and Hamner 1988). Eddies and wakes might function as retention belts for eggs and larvae (Caldeira *et al.* 2001). Plankton communities around Santa Catalina Island's shelf are significantly different from plankton communities away from shore, in deeper oceanic waters (Caldeira *et al.* Island-induced (meso)zooplankton communities: a case study around Santa Catalina Island, Southern California Bight, manuscript in preparation, 2005). As eddies are generated through a variety of mechanisms in the SCB, future studies should work towards distinguishing between the types of eddies observed in model output and satellite imagery in order to better understand their properties and potential impacts.

As suggested by Bray *et al.* (1999), there are local and remote wind forcing circulation patterns in the SCB that can only be resolved with a wind-driven model for the whole region. The one-way nesting procedure used AGRIF extensively described in (Blayo and Debreu 1999) enabled for an increase in eddy-kinetic-energy resolved in the child model (2.2 km) which became crucial in resolving the detailed island wake activity around Santa Catalina Island. Further details of the embedded method used in ROMS will be discussed elsewhere. Also, Bray *et al.* (1999) showed, that poleward flow in the SCB is maximum in the winter and summer and that there is an equatorial anomaly in the alongshore current associated with a wind stress during spring.

### **Submesoscale dynamics and time series analysis**

More anticyclonic features were observed in the ROMS solutions than in the SAR imagery. These differences are potentially attributable to a number of factors. First, the resolution of the SAR imagery (~100 m) is significantly greater than that of ROMS solutions (2 km). Also, observations of larger eddies may be effectively limited by the size of the ERS-1/2 SAR images (100 km<sup>2</sup>), potentially skewing the relative abundance toward smaller eddy classes. Regarding the relative distribution of cyclonic versus anticyclonic eddies, the submesoscale eddies observed in the SAR study were primarily of the "spiral" variety as described in Munk *et al.* (2000). This latter study indicated that surfactants might preferentially concentrate within cyclonic convergence zones, thereby potentially allowing spiral eddies to be visualized more readily (e.g., in SAR

images) than anticyclonic eddies. However, the authors also noted that cyclonic rotation in spiral eddies is favored for numerous reasons; that is, shear, static, centrifugal, and inertial instabilities can limit anticyclonic development. In this context, the physical properties of an eddy (e.g., size, rotational sense, vertical structure and surface signatures related to temperature or roughness) can vary depending upon the type or class of the eddy being observed.

The SCB region, because of its bathymetric configuration is obviously very complex and island-induced wakes are frequent. These cannot be resolved from long-term average data. Eddies in our simulations and observations are short-lived around Santa Catalina Island (3 - 7 days). Because of their frequent occurrences they must have important effects in overall poleward and equatorward transport in the San Pedro Basin, with implications for nutrient flux, productivity, plankton patchiness, larval transport and recruitment and dispersal of pollutants (DiGiacomo and Holt 2001). Seasonally, these authors found, most eddy activity around Santa Catalina Island occurred during winter. Winter is also a seasonal maximum for the Southern California Counter Current (Hickey 1992, 1998). Therefore strong poleward transport may frequently foster the formation of small-scale eddies around headlands and islands in the SCB.

Prior discussions on the mesoscale phenomena of the SCB have overlooked the importance of island wakes (Hickey 1979, 1991, 1992, 1993, 1998; Bray *et al.* 1999). Wind and current wakes are also generated by other islands of the SCB and their relative importance and interaction require further attention. Future work should consider the use of integrated multi-sensor (e.g., ocean color, SAR, SST) approaches, using single (e.g., ENVISAT) or multiple platforms, to identify small-scale island-generated features in the SCB and elsewhere.

Time-series analysis suggests that there is a concurrence of low SST with increases in sea surface chlorophyll around Santa Catalina, San Clement and San Nicholas Islands, indicating island mass effect. The seasonality of such events suggests that they might be related to the seasonality of the CC and CCC. Further studies should use numerical simulations in conjunction with *in situ* data to determine the forcing mechanisms that modulate the seasonality of the CC and CCC and determine their effect in the formation of island wakes in the SCB.

## LITERATURE CITED

- Caldeira, R.M.A., P. Russell and A. Amorim. 2001. Evidence of an unproductive coastal front in Baía D'Abra, an embayment on the south east of Madeira Island, Portugal. *Bulletin of Marine Science* 69:1057-1072.
- Caldeira, R.M.A., S. Groom, P. Miller, D. Pilgrim and N.P. Nezlin. 2002. Sea-surface signatures of the island mass effect phenomena around Madeira Island, Northeast Atlantic. *Remote Sensing of Environment* 80:336-360.
- Chavez, F.P. 1995. A comparison of ship and satellite chlorophyll from California and Peru. *Journal of Geophysical Research* 100-24:855-24,862.
- Clemente-Colon, P. and X.H. Yan. 2000. Low backscatter ocean features in synthetic aperture radar imagery. *John Hopkins APL Technical Digest* 21:116-121.
- Coutis, P. and J. Middleton. 1999. Flow-topography interaction in the vicinity of an isolated, deep ocean island. *Deep-Sea Research Part I Oceanographic Research Papers* 46:1633-1652.
- Dietrich, D., M. Bowman, C. Lin and A. Mestas-Nunez. 1996. Numerical studies of small island wakes. *Geophysics Astrophysics and Fluid Dynamics* 83:195-231.
- DiGiacomo, P.M. and B. Holt. 2001. Satellite observations of small coastal ocean eddies in the Southern California Bight. *Journal of Geophysical Research* 106:22,521-22,544.
- DiGiacomo, P.M., L. Washburn, B. Holt and B. Jones. 2004. Coastal pollution hazards in Southern California observed by SAR imagery: stormwater plumes, wastewater plumes, and natural hydrocarbon seeps. *Marine Pollution Bulletin* 49:1013-1024.
- Doty, L. and M. Oguri. 1956. The island mass effect. *Journal du Conseil permanente internationale pour l'Exploration de la Mer* 22:33-37.
- Furukawa, K. and E. Wolanski. 1998. Shallow-water frictional effects in island wakes. *Estuarine Coastal and Shelf Science* 46:599-608.

- Hamner, W. and I. Hauri. 1981a. Effects of island mass: water flow and plankton pattern around a reef in the Great Barrier Reef lagoon, Australia. *Limnology and Oceanography* 26:1084-1102.
- Hamner, W. and I. Hauri. 1981b. Long-distance horizontal migrations of zooplankton (*Scyphomedusae: Mastigias*). *Limnology and Oceanography* 26:414-423.
- Haney, R., R. Hale and D. Dietrich. 2001. Offshore propagation of eddy kinetic energy in the California Current. *Journal of Geophysical Research* 106:11,709-11,717.
- Hernandez-Leon, S. 1988. Gradients of mesozooplankton biomass and ETS activity in the wind-shear area as evidence of an island mass effect in the Canary Island waters. *Journal of Plankton Research* 10:1141-1154.
- Hernandez-Leon, S. 1991. Accumulation of mesozooplankton in a wake area as a causative mechanism of the "island-mass effect". *Marine Biology* 109:141-147.
- Hickey, B.M. 1979. The California Current system-hypotheses and facts. *Progress in Oceanography* 8:191-279.
- Hickey, B.M. 1991. Variability in two deep coastal basins (Santa Monica and San Pedro) off Southern California. *Journal of Geophysical Research* 96:16,689-16,708.
- Hickey, B.M. 1992. Circulation over the Santa Monica-San Pedro basin and shelf. *Progress in Oceanography* 30:37-115.
- Hickey, B.M. 1993. Physical oceanography. pp. 19-70 in: M.D. Dailey, D. Reish and J. Anderson (eds.), *Ecology of the Southern California Bight*. University of California Press. Berkeley, CA.
- Hickey, B.M. 1998. Coastal oceanography of Western North America from the tip of Baja California to Vancouver Island. pp. 345-393 in: A.R. Robinson and K.H. Brink (eds.), *The Sea*, Vol. 11. John Wiley. New York, NY.
- Imberger, J. 1985. The diurnal mixed layer. *Limnology and Oceanography* 30:737- 770.
- Joint Panel on Oceanographic Tables and Standards. 1991. Processing of oceanographic station data report. United Nations Education, Science and Culture Organization. Paris, France.
- Lynn, R. and J. Simpson. 1987. The California Current System: the seasonal variability of its physical characteristics. *Journal of Geophysical Research* 92:12,947-12,966.
- Marchesiello, P., J.C. McWilliams and A. Shchepetkin. 2001. Open boundary conditions for long-term integration of regional oceanic models. *Ocean Modeling* 3:1-20.
- Marchesiello, P., J.C. McWilliams and A. Shchepetkin. 2003. Equilibrium structure and dynamics of the California Current System. *Journal of Physical Oceanography* 33:753-783.
- McClain, E., W. Pichel and C. Walton. 1985. Comparative performance of AVHRR-based multi-channel sea surface temperatures. *Journal of Geophysical Research* 90:11,587-11,601.
- Munk, W., K.L. Armi, F. Fischer and A. Zachariasen. 2000. Spirals on the sea. *Proceedings of the Royal Society London, Series A* 456:1217-1280.
- Owen, R.W. 1980. Eddies of the California current system: physical and ecological characteristics. pp. 237-263 in: D.M. Power (ed.), *The California Islands: Proceedings of a Multidisciplinary Symposium*. Santa Barbara Museum of Natural History. Santa Barbara, CA.
- Penven, P., L. Debreu, P. Marchesiello and J.C. McWilliams. 2006. Evaluation and application of the ROMS 1-way embedding procedure to the central California upwelling system. *Ocean Modelling* 12:157-187.
- Reid, J. and A.W. Mantyla. 1976. The effect of the geostrophic flow upon coastal sea elevations in the northern North Pacific ocean. *Journal of Geophysical Research* 81:31,000-3110.
- Rissik, D., I.M. Suthers and C.T. Taggart. 1997. Enhanced particle abundance in the lee of an isolated reef in the south Coral Sea: the role of flow disturbance. *Journal of Plankton Research* 19:1347-1368.

Robinson, I.S. 2004. Measuring the Oceans from Space : The Principles and Methods of Satellite Oceanography. Springer, Berlin.

Shchepetkin, A. and J.C. McWilliams. 1998. Quasi-monotone advection schemes based on explicit locally adaptive dissipation. *Monthly Weather Review* 126:1541-1580.

Shchepetkin, A. and J.C. Mc Williams. 2003. A method for computing horizontal pressure-gradient force in an ocean model with a non-aligned vertical coordinate. *Journal of Geophysical Research* 108:3090.

Shchepetkin, A. and J.C. Mc Williams. 2005. The Regional Oceanic Modeling System (ROMS): A split-explicit, free-surface, topography-following-coordinate oceanic model. *Ocean Modelling* 9:347-404.

Smith, R.C. and K. Baker. 1978. The bio-optical state of ocean waters and remote sensing. *Limnology and Oceanography* 23:247-259.

Sverdrup, H. and R. Fleming. 1941. The waters off the coast of Southern California, March to July 1937. *Bulletin of the Scripps Institution of Oceanography* 4:261-378.

Tomczak, M. and J. Godfrey. 1994. Regional Oceanography: An Introduction. Elsevier Science. New York, NY.

Walton, C. 1988. Non-linear multichannel algorithms for estimating sea surface temperature with AVHRR satellite data. *Journal of Applied Meteorology* 27:115-124.

Winant, C.D., D.J. Alden, E.P. Dever, K.A. Edwards and M.C. Hendershott. 1999. Near-surface trajectories off central and Southern California. *Journal of Geophysical Research* 104:15,713-15,726.

Wolanski, E. and W. Hamner. 1988. Topographically controlled fronts in the ocean and their biological influence. *Science* 241:177-181.  
Wolanski, E., J. Imberger and M. Heron. 1984. Island wakes in shallow coastal waters. *Journal of Geophysical Research* 89:10, 553-10,569.

Wolanski, E., T. Asaeda, A. Tanaka and E. Deleersnijder. 1996. Three-dimensional island wakes in the field, laboratory experiments and numerical models. *Continental Shelf Research* 16:1437-1452.

## ACKNOWLEDGMENTS

We wish to acknowledge William Hamner and Peggy Fong for their editorial comments to early versions of the manuscript. We also wish to thank Renee Maabadi for helping with the processing of CTD data. We thank Ben Holt for assisting with the SAR data acquisition and interpretation, and Clint Winant for supplying the Santa Barbara Channel drifter data. The JPL effort was supported by the National Aeronautics and Space Administration through a contract with the Jet Propulsion Laboratory, California Institute of Technology. R.M.A. Caldeira was supported by a PhD scholarship from the Madeira Education Secretariat (POPRAM II/III). We are also greatly indebted to anonymous reviewers for their suggestions.